Converting capsules to sensors for nondestructive analysis

Zhang, Yan; Zhang, Zhibing; Ding, Yulong; Pikramenou, Zoe; Li, Yongliang

DOI:
10.1021/acsami.8b17679

Converting Capsules to Sensors for Nondestructive Analysis: From Cargo-Responsive Self-Sensing to Functional Characterization

Yan Zhang,[†,‡] Zhibing Zhang,[‡] Yulong Ding,[†] Zoe Pikramenou,[§] Yongliang Li*[†]*

[†] Birmingham Center for Energy Storage, School of Chemical Engineering, University of Birmingham, Edgbaston, Birmingham, West Midlands, B15 2TT, United Kingdom

[‡] Micromanipulation and Microencapsulation Research Group, School of Chemical Engineering, University of Birmingham, Edgbaston, Birmingham, West Midlands, B15 2TT, United Kingdom

[§] Photophysics Group, School of Chemistry, University of Birmingham, Edgbaston, Birmingham, West Midlands, B15 2TT, United Kingdom

KEYWORDS: retention, leakage, capsule, sensor, fluorescence, nondestructive, phase change materials, thermal energy storage

ABSTRACT A general concept of converting capsules into sensors is reported. Such simple conversion enables instantaneous nondestructive analysis for applications such as controlled release and energy storage among others. Converted capsule sensors are responsive in emission colors to varying core cargos via the incorporation of a solvatochromic fluorophore under excitation. Such cargo-responsive self-sensing abilities facilitate their application in capsule-level analysis such as cargo retention-leakage detection and release implications, as well as

defect identification. The versatile concept is shown as an auxiliary tool in thermal energy storage to visualize phase transition, exhibiting promising potentials in application-level characterization.

Encapsulation is a technique to enclose functional cargos within a wrapping shell for protection and controlled release, widely used in food and pharmaceuticals,[1-3] fragrances,[4] self-healing materials,[5] batteries,[6] and energy storage.[7-8] Regardless of targeted applications, the first and foremost characterization required is on the capsule level pertaining to the retention and release of encapsulated cargos. Common techniques, such as UV-Vis spectroscopy and differential scanning calorimetry (DSC), either require destructive extraction of core analytes or are inadequate to deliver cost-effective analysis when quantification is not necessary. An expeditious technique for fast-tracking capsule quality is long overdue, yet still lacking in both academia and industry. We hereby bridge the gap by proposing a simple, fast and effective nondestructive concept of bestowing capsules with sensing abilities using fluorophores to deliver the aforementioned objective. Fluorophores have been utilized in encapsulation for imaging and shell thickness measurement,[9-13] but neither for analysis reported here nor on the same principle. Our developed concept entails one extra step of integrating a fluorophore into existing formulation protocols and no further sample preparation for characterization. The application realm of such a versatile methodology surprisingly advances far beyond the initial intention.

Many fluorophores are eminently fluorescent in organic solvents, but subject to solvatochromism. They emit photons of different wavelengths in response to their solvent environments, owing to a change in charge distribution upon interaction with the solvent molecules.[14-15] If a fluorophore features distinctive emission wavelengths under excitation in

solvents from in air, color switching is expected as its surrounding environment changes from liquid to gas. We speculate that this concept can be exploited as a nondestructive method to confirm retention and detect leakage of core cargos.

To prove the assertion, a common fluorophore Nile red was selected as a staining agent. While its excitation maximum lies within the blue region on the visible spectrum, a red emission color was observed in air. The large Stokes shift of the fluorophore allows for a potential discernible color switch when its environment changes. As a proof of concept, a variety of Nile red stained chemicals ranging from hydrocarbons to esters and alcohols, representing the miscellaneous cargos of interest for diverse applications, was encapsulated as shown in Figure 1 (a). With most nonhalogenated hydrocarbons bearing a normalized solvent polarity parameter E_T^N in the lower range (0.006~0.015 for aliphatic hydrocarbons and 0.068~0.111 for arenes) on the empirical spectroscopically-derived $E_T(30)$ scale, and its gradual increase to 0.194~0.577 for esters and 0.222~1.068 for alcohols,[16] a polarity increase from hydrocarbons to alcohols is generally recognized. The relative permittivity ε_r of each cargo calculated following a reported equation[17] further confirmed explicitly their polarity disparity (Figure 1 (b)). These suggest a polarity-induced solvatochromism nature in the distinct emission colors of capsules with selected cargos spanning the visible spectrum.

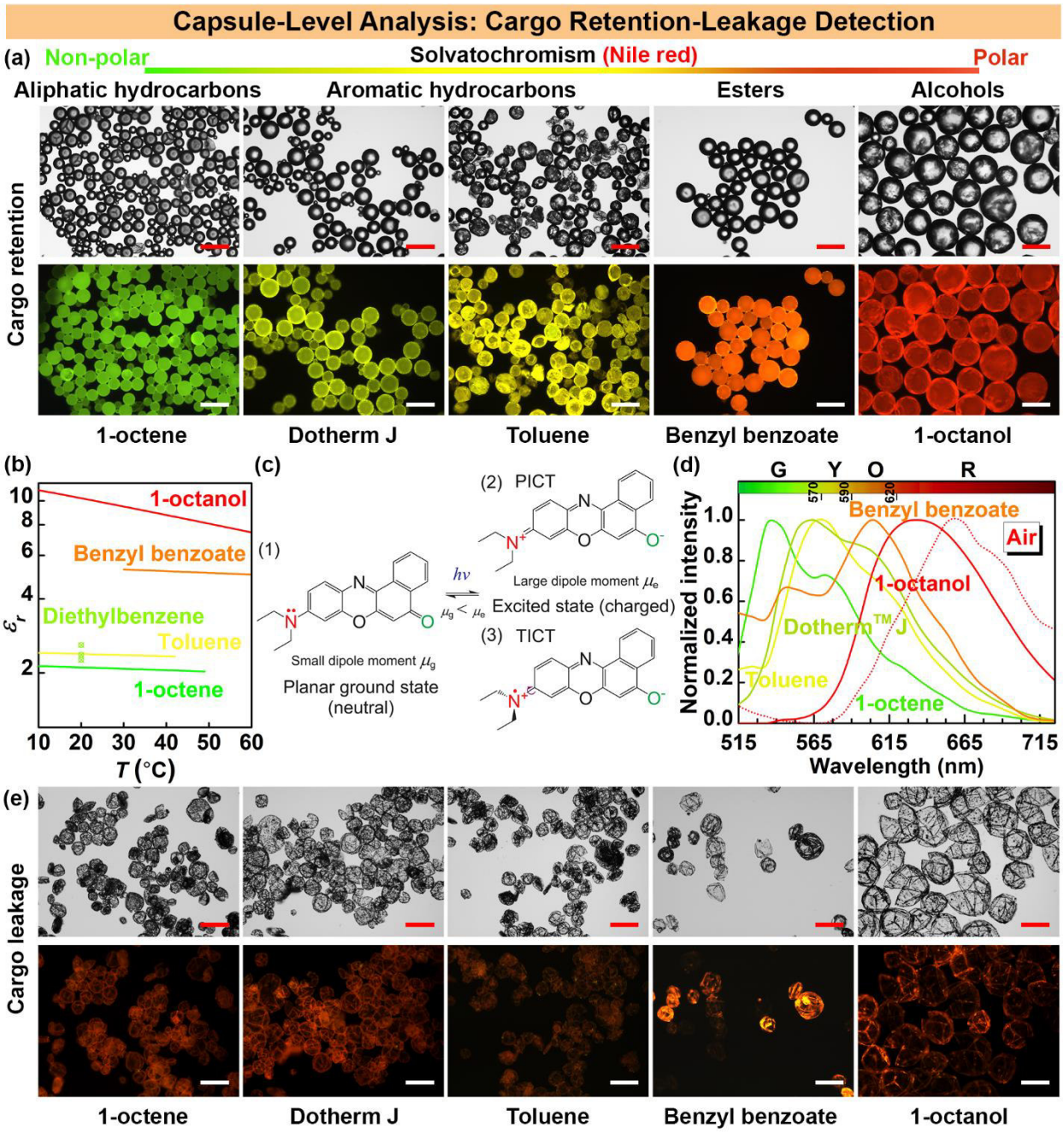

Figure 1 Capsule-level analysis: cargo retention-leakage detection. (a) Bright-field optical and fluorescence microscopy images (scale bars 100 µm) of dry poly(urea formaldehyde) (PUF) capsules loaded with various Nile red stained organic core cargos (1-octene, Dotherm J, toluene, benzyl benzoate and 1-octanol) produced by gum Arabic as the emulsifier showing a bathochromic emission shift with increasing cargo polarity under excitation by a blue light (excitation wavelength maximum $\lambda_{ex\ max}$ = 460 nm); (b) calculated relative permittivity ε_r for selected core cargos. Dotherm J is an aromatic hydrocarbon mixture with its principal ingredient being diethylbenzene. Calculation was performed with all three isomers ortho-, meta, para-dimethylbenzene, and results are denoted by three circles crossed in the center; (c) the neutral ground state of Nile red and its two possible resonance forms, twisted intramolecular charge transfer (TICT) and planar intramolecular charge transfer (PICT), in the charged excited state; (d) normalized fluorescence emission spectra (monochromatic excitation laser wavelength λ_{ex} = 488 nm) of capsules loaded with the above-

mentioned cargos stained by Nile red; (e) bright-field and fluorescence microscopy images (scale bars 100 µm) of crushed PUF capsules with the miscellaneous cargos in (a) dried after 72 h.

The resonance form of excited Nile red in solvents has been attributed to either twisted intramolecular charge transfer (TICT) or planar intramolecular charge transfer (PICT) configurations (Figure 1 (c)), though more research evidence is supporting the latter.[18-23] Despite its precise resonance form in dispute, the positive solvatochromism of Nile red confers a larger dipole moment to the charged Franck-Condon excited state (μ_e) than to the neutral ground state (μ_g). The latter is better stabilized by nonpolar solvents, when the delocalization of electrons from the amine donor to the carbonyl acceptor alters the electron distribution within the fluorophore.[15, 24] The alkene-loaded capsules effused a green fluorescent color corresponding to the energy discrepancy between different states on the Jablonski diagram following the fluorophore's photon emission, and its wavelength underwent a bathochromic (red) shift as the cargo varied from a low-ε_r nonpolar hydrocarbon to a high-ε_r polar alcohol, in agreement with the fluorescence emission spectra presented in Figure 1 (d).

A perceptible color switch upon the solvation-nonsolvation of Nile red, corresponding to cargo retention-leakage, was particularly anticipated for nonpolar cargos. The resembling red tones of unloaded capsules after rupture for accelerated release (Figure 1 (e)), independent of their original colors (Figure 1 (a)), confirmed this speculation. The cargo retention-leakage color indication was green-red, lime-red and yellow-red for 1-octene, Dotherm J, and toluene respectively. The larger Stokes shift of Nile red in more polar solvents separated its excitation and emission maxima further apart, pushing its emission wavelength closer to that in air. The color switch contrast diminished substantially as a result, and became nearly indistinguishable for benzyl benzoate and 1-octanol, compromising the feasibility of using Nile red as an indicator. It should be noted, however, that the extremely low volatility of benzyl benzoate inflicted

enduring interaction between its residual molecules and Nile red, obstructing an otherwise plausible orange-red color switch. By encapsulating a more volatile ester alternative, isobutyl acetate, an orange-red color switch did reveal as expected (Figure S1). The contrast was genuinely lost for Nile red in 1-octanol, ascribable to emitted photons of similar wavelengths in both air and the alcohol. Nonetheless, we substituted a negatively solvatochromic Brooker's merocyanine dye (MOED) for Nile red and repeated the experiment with 1-octanol. Results (Figure S2) demonstrated that restoring the color switch for retention-leakage indication of polar alcohols was successful by resorting to a different fluorophore.

These results proved that appropriately selected fluorophores can be incorporated in core cargos to bestow capsules with retention-leakage self-sensing abilities. As a general guidance, the soluble fluorophores selected must emit photons of distinct wavelengths in the encapsulated cargos from in air, corresponding to discernible colors on the visible spectrum. Capsule defects such as trapped bubbles can also be easily recognized (Figure S3). Such capsule-level analysis enables more rapid and efficient materials screening and parameter optimization for synthesis during the initial research and development stage.

Interestingly, permeability of capsule shells can also be insinuated from the time scale of the fluorescent color change and the remaining percentage of highly fluorescent capsules. We use samples of different release behaviors imparted by various emulsifiers for demonstration here (Figure S4). Figure 2 (a) presents highly permeable capsules with a fast release profile, manifested by the rapid dimming of the initial highly fluorescent green color. The 1 min aliquot captured the incomplete rapid leaking, comprising both highly bright and dim regions (gray values shown in Figure S5) corresponding to loaded and unloaded capsules, respectively. Residual heptane was quantified by gas chromatography with a mass spectrometer detector (GC-

MS) to be approximately 0.35 ± 0.06 *wt.%* when freshly dried, while no GC response was returned after 72 h implying a complete cargo loss. Batch 2 (Figure 2 (b)) suffered substantial leakage but at a much slower rate, whereas batch 3 (Figure 2 (c)) had the slowest release. Good agreement with thermogravimetric analysis (TGA) (Figure 2 (d)) suggests the feasibility of using the concept as an alternative for qualitative release behavior cross-comparison, when detailed quantification is not required. This could be of potential importance for controlled release in drug design, food flavors, detergents and cosmetics products such as perfume.

Versatility of this concept not only enables nondestructive analysis of capsules, but also provides insights into the encapsulation process itself. For instance, solvent extraction relies on a volatile good solvent to dissolve the shell and core materials into a one-phase mixture and subsequent evaporation of the solvent to induce shell precipitation engulfing the core. [25-27] Convoluted interfacial tension study and tertiary phase diagram sketching are usually required to guarantee fully engulfed core-shell structured capsules.[26] Alternatively, capsule structures can be easily confirmed with this developed concept (see Figure S6 in Supporting Information for more details).

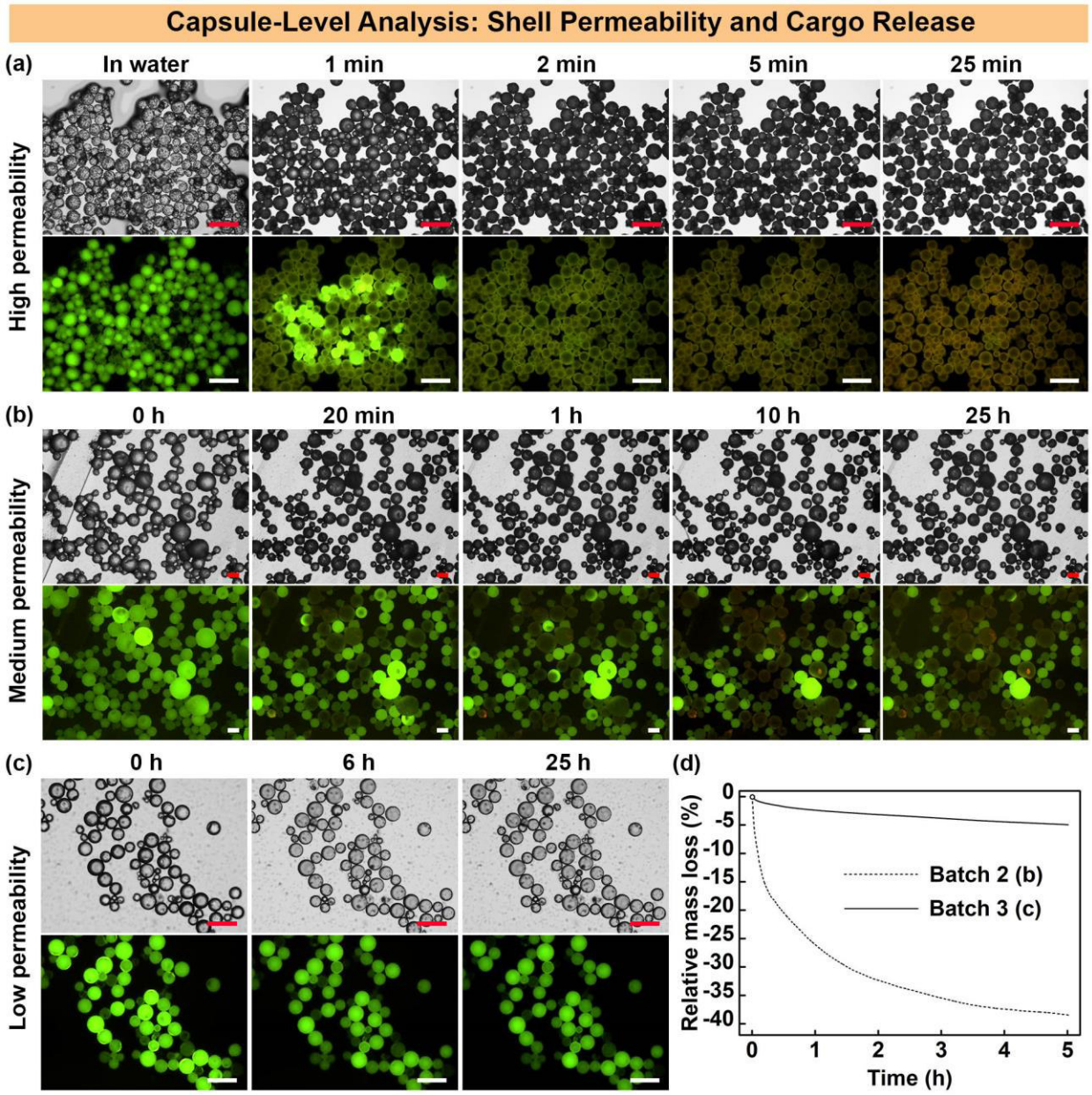

Figure 2 Capsule-level analysis: shell permeability and cargo release. Time-resolved images (scale bars 100 µm) of Nile red stained heptane-PUF capsules with (a) high shell permeability (fast release, poly(vinyl alcohol) as the emulsifier), (b) medium shell permeability (intermediate release, gelatin-grafted graphene oxide as the emulsifier), and (c) low shell permeability (slow release, gelatin as the emulsifier); (d) relative mass loss of capsules with medium (batch 2 (b)) and low (batch 3 (c)) permeability recorded by TGA in agreement with implications from fluorescence microscopy study in (a) - (c) (batch 1 (a) was not investigated by TGA due to the drastically fast leakage).

We have demonstrated so far that capsule-level analysis can be achieved with great ease following our concept. The immediate results assist chemists and materials scientists innovating upstream at front-end synthesis by reducing development time and minimizing disruption to

formulation, when evitable quantification would lengthen and complicate the process otherwise. Surprisingly, we succeeded in demonstrating that our concept can even provide insights to application-level characterization, using the example of phase transition visualization of paraffin-based phase change materials (PCMs) in thermal energy storage. DSC thermogram of encapsulated hexadecane in Figure 3 (a) revealed two separate phase transition temperature peaks at 6.5 ± 0.2 ℃ for exothermic cooling (blue point ③ on the DSC thermogram in Figure 3 (a)) and 20.9 ± 0.2 ℃ for endothermic heating (blue point ⑥), respectively. Noncoalescence of the two peaks, featuring a lower nucleation temperature during exothermic cooling, indicated the typical presence of supercooling (ΔT = 14.4 ± 0.3 ℃). DSC offers quantification of thermal properties such as enthalpy of fusion and phase change temperatures. Phase change onsets have to be estimated by defining a threshold of the first-order derivative of heat flow with respective to time. Fluorescent sensing, on the other hand, assists in direct visualization of this process with good accuracy.

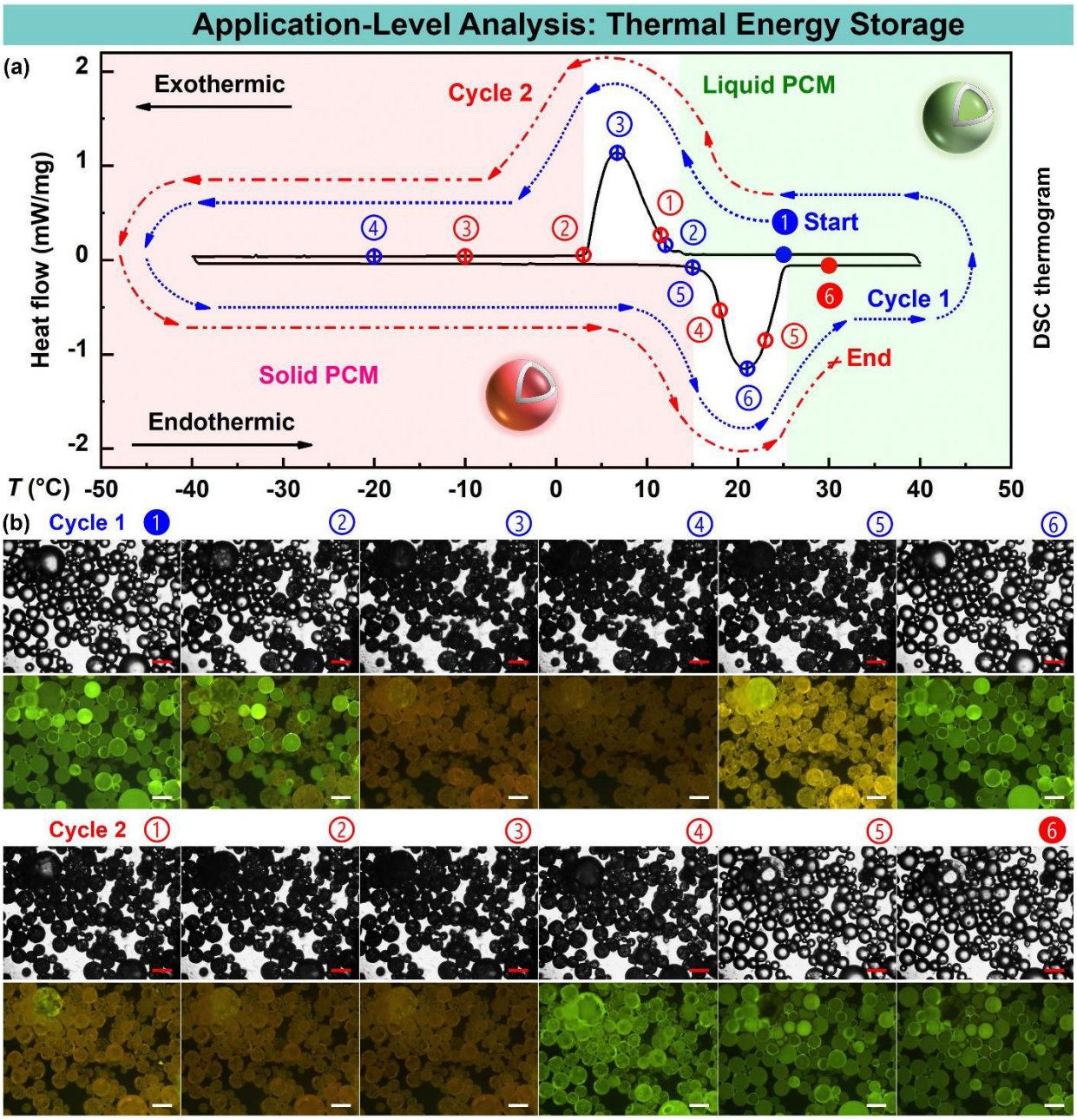

Figure 3 Application-level analysis: thermal energy storage. (a) DSC thermogram of hexadecane-PUF capsules produced with xanthan gum as the emulsifier showing two separate phase change temperature peaks during exothermic cooling and endothermic heating; (b) microscopy micrographs (scale bars 100 µm) of the same hexadecane-PUF capsules in a Linkam cooling chamber at temperatures denoted on the DSC thermogram demonstrating subtle light transmission change (bright-field microscopy) and pronounced color switch upon phase transition (fluorescence microscopy) for two thermal cycles.

A change in the refractive index of hexadecane owing to its phase transition induced subtle contrast in light transmission. Capsules with liquid cores consequently appeared heterogeneously

bright in the center surrounded by a dark periphery, but homogeneously dark for those with solid cores under bright-field microscopy (Figure 3 (b)). A fluorescent color switch significantly highlighted phase transition. The order of color change for the exothermic and endothermic processes was primarily from green to orange and then back to green again, in synchronization with the liquid-solid-liquid phase change of hexadecane. When hexadecane was in the liquid form, destabilization of Nile red's excited state with a large dipole moment in the nonpolar PCM caused the solvated fluorophore to emit photons of a shorter wavelength in the green spectrum. When hexadecane crystalized, Nile red became gradually nonsolvated by the solid hexadecane starting from the onset of its phase change, analogous to excitation in air. The emission color of frozen capsules deviated from a red to a dark orange tone. This attributes to the hypsochromic (blue) shift of emission maxima for fluorophores on account of lowering temperature.[28-30]

Upon transition between the solid and liquid states of the PCM, the fluorophore functioned as a reversible phase transition sensor. Reversibility was confirmed by consistent color switching shown in the fluorescence micrographs within the two separate thermal cycles denoted on the DSC thermogram. The appearing yellow color at blue points ② (12.0 ℃ from cooling stage reading) and ⑤ (15.0 ℃ from cooling stage reading) during cycle 1 demonstrated not only the proficiency of detecting the solid-liquid states of the PCM, but also the aptitude of identifying phase transition onsets (11.7 ± 0.1 ℃ and 15.1 ± 0.1 ℃ from DSC results). This greatly facilitates crystallization and supercooling study in thermal energy storage with the auxiliary capability of visualization. Downstream engineers working in back-end application fields can also become beneficiaries of such a concept for advantages unavailable from conventional characterization techniques.

We conceived and demonstrated in this work a concept of bestowing sensing abilities to capsules via fluorescent staining. This concept takes advantage of the solvatochromism phenomenon, which requires only dissolution of selected fluorophores into core cargos. Reaction chemistry to bind fluorophores via functional moieties as in bioscience imaging is not demanded. No noticeable effect on the encapsulation process itself such as yield owing to incorporating fluorophores was recognized. Converted sensor capsules can rapidly distinguish between real capsules and other camouflage forms such as solid or hollow particles. The great ease of achieving instantaneous results not only provides a long overdue solution to fast capsule inspection, but also promotes the methodology as an effective tool for studies above the capsule-level. The concept is expected to be applicable to all encapsulation routes such as in situ and interfacial polymerization, gelation, microfluidics, coacervation and solvent extraction upon selecting appropriate fluorophores. Most intriguingly, we utilized the synchronization between Nile red solvation-nonsolvation by hexadecane and the liquid-solid states of the hydrocarbon to successfully visualize the phase transition of an encapsulated paraffin-based PCM. Capsules converted in this way function as reversible phase transition indicators themselves potentially for crystallization and super-cooling study in thermal energy storage research. We speculate that the versatile concept, proved useful for both capsule-level and application-level analysis, can be of interest and benefit for other fields.

ASSOCIATE CONTENT

Supporting Information

The Supporting Information is available free of charge on the ACS Publications website at DOI:

Experimental section detailing materials, capsules synthesis, and characterization techniques, and results and discussion (PDF)

AUTHOR INFORMATION

Corresponding Authors

* E-mail: Z.Zhang@bham.ac.uk (Z.Z.)

* E-mail: Y.Li.1@bham.ac.uk (Y.L.)

ORCID

Yan Zhang: 0000-0003-4752-877X

Zhibing Zhang: 0000-0003-2797-9098

Zoe Pikramenou: 0000-0002-6001-1380

Yongliang Li: 0000-0001-6231-015X

Notes

The authors declare no competing financial interest.

Author Contributions

Yan Zhang designed and performed the experiments, analyzed experimental data and drafted the manuscript. Zoe Pikramenou contributed to the selection of an appropriate negatively solvatochromic fluorophore. Zhibing Zhang, Yulong Ding and Yongliang Li provided suggestions to this work. All authors made comments on the manuscript.

Funding Sources

This work is funded by the Engineering and Physical Sciences Research Council (EPSRC) in the U.K. (EP/N000714/1 and EP/N021142/1).

ACKNOWLEDGMENT

The authors would like to express their gratitude to EPSRC for the funding provided, and to Dr. Alessandro Di Maio from School of Biosciences, Dr. Christopher Stark from School of Geography, Earth and Environmental Studies, Dr. James Andrews, Ms Jie Chen and Miss Anabel Trujillo from School of Chemical Engineering at University of Birmingham for their generous support.

REFERENCES

(1) Champagne, C. P.; Fustier, P. Microencapsulation for the Improved Delivery of Bioactive Compounds into Foods. *Curr. Opin. Biotechnol.* **2007,** *18* (2), 184-190.

(2) Agnihotri, S. A.; Mallikarjuna, N. N.; Aminabhavi, T. M. Recent Advances on Chitosan-Based Micro- and Nanoparticles in Drug Delivery. *J. Controlled Release* **2004,** *100* (1), 5-28.

(3) Horcajada, P.; Chalati, T.; Serre, C.; Gillet, B.; Sebrie, C.; Baati, T.; Eubank, J. F.; Heurtaux, D.; Clayette, P.; Kreuz, C.; Chang, J.-S.; Hwang, Y. K.; Marsaud, V.; Bories, P.-N.; Cynober, L.; Gil, S.; Férey, G.; Couvreur, P.; Gref, R. Porous Metal–Organic-Framework Nanoscale Carriers as a Potential Platform for Drug Delivery and Imaging. *Nat. Mater.* **2009,** *9*, 172.

(4) Sadovoy, A. V.; Lomova, M. V.; Antipina, M. N.; Braun, N. A.; Sukhorukov, G. B.; Kiryukhin, M. V. Layer-by-Layer Assembled Multilayer Shells for Encapsulation and Release of Fragrance. *ACS Appl. Mater. Interfaces* **2013,** *5* (18), 8948-8954.

(5) Song, Y.-K.; Jo, Y.-H.; Lim, Y.-J.; Cho, S.-Y.; Yu, H.-C.; Ryu, B.-C.; Lee, S.-I.; Chung, C.-M. Sunlight-Induced Self-Healing of a Microcapsule-Type Protective Coating. *ACS Appl. Mater. Interfaces* **2013,** *5* (4), 1378-1384.

(6) Lim, T.-W.; Park, C. W.; White, S. R.; Sottos, N. R. Time Release of Encapsulated Additives for Enhanced Performance of Lithium-Ion Batteries. *ACS Appl. Mater. Interfaces* **2017,** *9* (46), 40244-40251.

(7) Zheng, Z.; Chang, Z.; Xu, G.-K.; McBride, F.; Ho, A.; Zhuola, Z.; Michailidis, M.; Li, W.; Raval, R.; Akhtar, R.; Shchukin, D. Microencapsulated Phase Change Materials in Solar-Thermal Conversion Systems: Understanding Geometry-Dependent Heating Efficiency and System Reliability. *ACS Nano* **2017,** *11* (1), 721-729.

(8) Yoo, Y.; Martinez, C.; Youngblood, J. P. Synthesis and Characterization of Microencapsulated Phase Change Materials with Poly(urea−urethane) Shells Containing Cellulose Nanocrystals. *ACS Appl. Mater. Interfaces* **2017,** *9* (37), 31763-31776.

(9) Lebedeva, O. V.; Kim, B.-S.; Vinogradova, O. I. Mechanical Properties of Polyelectrolyte-Filled Multilayer Microcapsules Studied by Atomic Force and Confocal Microscopy. *Langmuir* **2004,** *20* (24), 10685-10690.

(10) Chen, H.; Ouyang, W.; Lawuyi, B.; Prakash, S. Genipin Cross-Linked Alginate-Chitosan Microcapsules: Membrane Characterization and Optimization of Cross-Linking Reaction. *Biomacromolecules* **2006,** *7* (7), 2091-2098.

(11) Tavera, E. M.; Kadali, S. B.; Bagaria, H. G.; Liu, A. W.; Wong, M. S. Experimental and Modeling Analysis of Diffusive Release from Single‐Shell Microcapsules. *AIChE J.* **2009,** *55* (11), 2950-2965.

(12) Rigler, P.; Meier, W. Encapsulation of Fluorescent Molecules by Functionalized Polymeric Nanocontainers: Investigation by Confocal Fluorescence Imaging and Fluorescence Correlation Spectroscopy. *J. Am. Chem. Soc.* **2006,** *128* (1), 367-373.

(13) Sotoma, S.; Hsieh, F.-J.; Chen, Y.-W.; Tsai, P.-C.; Chang, H.-C. Highly Stable Lipid-Encapsulation of Fluorescent Nanodiamonds for Bioimaging Applications. *Chem. Commun.* **2018,** *54* (8), 1000-1003.

(14) Renger, T.; Grundkötter, B.; Madjet, M. E.-A.; Müh, F. Theory of Solvatochromic Shifts in Nonpolar Solvents Reveals a New Spectroscopic Rule. *Proc. Natl. Acad. Sci. U.S.A.* **2008,** *105* (36), 13235-13240.

(15) Vincent, M.; Maged, H. Nile Red and Nile Blue: Applications and Syntheses of Structural Analogues. *Chem. – Eur. J.* **2016,** *22* (39), 13764-13782.

(16) Reichardt, C. In *Solvents and Solvent Effects in Organic Chemistry*, 2nd ed; Ebel, H. F., Ed.; VCH Verlagsgesellschaft mbH: Weinheim, Germany, 1988; Chapter 7, pp 339-405.

(17) Wohlfarth, C. *CRC Handbook of Chemistry and Physics*, 85th ed; CRC Press: Boca Raton, FL, USA, 2005.

(18) Sarkar, N.; Das, K.; Nath, D. N.; Bhattacharyya, K. Twisted Charge Transfer Processes of Nile Red in Homogeneous Solutions and in Faujasite Zeolite. *Langmuir* **1994,** *10* (1), 326-329.

(19) Camargo Dias, L.; Custodio, R.; Pessine, F. B. T. Theoretical Studies of Nile Red by Ab Initio and Semiempirical Methods. *Chem. Phys. Lett.* **1999,** *302* (5), 505-510.

(20) Jose, J.; Burgess, K., Benzophenoxazine-Based Fluorescent Dyes for Labeling Biomolecules. *Tetrahedron* **2006,** *62* (48), 11021-11037.

(21) Kawski, A.; Bojarski, P.; Kukliński, B. Estimation of Ground- and Excited-State Dipole Moments of Nile Red Dye from Solvatochromic Effect on Absorption and Fluorescence Spectra. *Chem. Phys. Lett.* **2008,** *463* (4), 410-412.

(22) Owen Tuck, P.; Christopher Mawhinney, R.; Rappon, M. An Ab Initio and TD-DFT Study of Solvent Effect Contributions to the Electronic Spectrum of Nile Red. *Phys. Chem. Chem. Phys.* **2009,** *11* (22), 4471-4480.

(23) Guido, C. A.; Mennucci, B.; Jacquemin, D.; Adamo, C. Planar vs. Twisted Intramolecular Charge Transfer Mechanism in Nile Red: New Hints from Theory. *Phys. Chem. Chem. Phys.* **2010,** *12* (28), 8016-8023.

(24) Reichardt, C. Solvatochromic Dyes as Solvent Polarity Indicators. *Chem. Rev.* **1994,** *94* (8), 2319-2358.

(25) Torza, S.; Mason, S. G. Coalescence of Two Immiscible Liquid Drops. *Science* **1969,** *163* (3869), 813-814.

(26) Loxley, A.; Vincent, B., Preparation of Poly(methylmethacrylate) Microcapsules with Liquid Cores. *J. Colloid Interface Sci.* **1998,** *208* (1), 49-62.

(27) González, L.; Kostrzewska, M.; Baoguang, M.; Li, L.; Hansen, J. H.; Hvilsted, S.; Skov, A. L. Preparation and Characterization of Silicone Liquid Core/Polymer Shell Microcapsules via Internal Phase Separation. *Macromol. Mater. Eng.* **2014,** *299* (10), 1259-1267.

(28) Hoff, W. D.; Kwa, S. L. S.; Grondelle, R. v.; Hellingwerf, K. J. Low Temperature Absorbance and Fluorescence Spectroscopy of the Photoactive Yellow Protein from Ectothiorhodospira Halophila. *Photochem. Photobiol.* **1992,** *56* (4), 529-539.

(29) Abbyad, P.; Childs, W.; Shi, X.; Boxer, S. G. Dynamic Stokes Shift in Green Fluorescent Protein Variants. *Proc. Natl. Acad. Sci. U.S.A.* **2007,** *104* (51), 20189-20194.

(30) Piatkevich, K. D.; Malashkevich, V. N.; Morozova, K. S.; Nemkovich, N. A.; Almo, S. C.; Verkhusha, V. V. Extended Stokes Shift in Fluorescent Proteins: Chromophore–Protein Interactions in a Near-Infrared TagRFP675 Variant. *Sci. Rep.* **2013,** *3*, 1847.

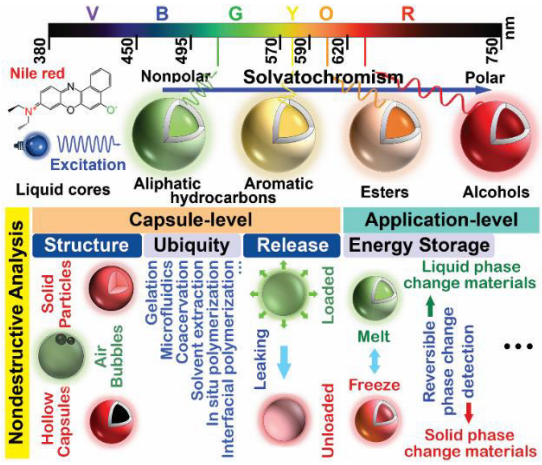

Graphic abstract

Supporting Information

Converting Capsules to Sensors for Nondestructive Analysis: From Cargo-Responsive Self-Sensing to Functional Characterization

Yan Zhang,[†‡] Zhibing Zhang,[‡] Yulong Ding,[†] Zoe Pikramenou,[§] Yongliang Li[*†]*

[†] Birmingham Center for Energy Storage, School of Chemical Engineering,

[‡] Micromanipulation and Microencapsulation Research Group, School of Chemical Engineering,

[§] Photophysics Group, School of Chemistry, University of Birmingham, Edgbaston, Birmingham, West Midlands, B15 2TT, United Kingdom

* Corresponding authors:

Prof. Zhibing Zhang

Tel: +44 (0)121 414 5334

Email: Z.Zhang@bham.ac.uk

Dr. Yongliang Li

Tel: +44 (0)121 414 5135

Email: Y.Li.1@bham.ac.uk

Experimental Section

***Materials*:** gum Arabic (Arcos Organics), gelatin (Sigma-Aldrich UK, G2500), graphene oxide nanocolloids (Sigma-Aldrich UK, 795534, 2 mg/mL, dispersed in H_2O), poly(vinyl alcohol) (Sigma-Aldrich UK, 363170, M_w 13,000~23,000, 87~89% hydrolyzed), poly(acrylic acid) (Sigma-Aldrich UK, 306215, average M_v ~ 1,250,000), xanthan gum from Xanthomonas campestris (Sigma-Alrich UK, G1253), (+)-arabinogalactan from larch wood (Sigma-Aldrich UK, 10830), sodium dodecyl sulfate (Sigma-Aldrich UK, 436143, ACS reagent, ≥ 99.0%), urea (Sigma-Aldrich UK, U5128, ACS reagent grade 99.0-100.5%), resorcinol (Sigma-Aldrich UK, 398047, ACS reagent, ≥99.0%), ammonium chloride (Sigma-Aldrich UK, A9434, for molecular biology, ≥99.5%), formaldehyde (Sigma-Aldrich UK, 47608, for molecular biology, BioReagent, ≥36.0% in H_2O), Nile red (Sigma-Aldrich UK, 72485), Brooker's merocyanine dye (Alfa Aesar, H66517), heptane (Sigma-Aldrich UK, 246654, anhydrous, 99%), 1-octene (Sigma-Aldrich UK, O4806, 98%), Dotherm J (Dow), toluene (Sigma-Aldrich UK, 244511, anhydrous, 99.8%), benzyl benzoate (Sigma-Aldrich UK, B6630, ReagentPlus®, ≥99.0%), isobutyl acetate (Sigma-Aldrich UK, W217506, ≥98%), 1-octanol (Sigma-Aldrich UK, 297887, anhydrous, ≥ 99.0%), hexadecane (Sigma-Aldrich UK, H6703, ReagentPlus®, 99%), dichloromethane (Sigma-Aldrich UK, 270997, anhydrous, ≥99.8%), and poly(methyl methacrylate) (Sigma-Aldrich UK, 445746, M_w 350,000).

***Capsule Synthesis – In Situ Polymerization*:** all amino resin capsules were synthesized via the one-step in situ polymerization process following an identical protocol unless specified otherwise. Modifications made to this protocol to produce the miscellaneous samples presented in the manuscript are described in details after the protocol. In most cases, modifications were mainly changing emulsifiers and how they were dissolved in water, in addition to core cargos. Amino resin capsules formulated via the one-step in situ polymerization are referred to as core-PUF capsules in the manuscript. For instance, heptane-PUF corresponds to capsules with heptane as the core and poly (urea formaldehyde) as the shell material. The standard protocol used throughout this work is as follows: **(1) *emulsifier solution preparation*:** the selected emulsifier is dissolved into 150 g (Mettler PM600 balance, 200 mL glass beaker) distilled water (conductivity ≤ 2.00 µS/cm, Mettler Toledo SevenCompact conductivity meter, InLab® 731 ISM electrode) at a specific concentration (Sartorius Secura124-1S analytical balance) to form a clear solution. Methods adopted to dissolve them and concentrations are individually specified following the

protocol; **(2)** ***additives and pH adjustment*****:** 2.500 g urea, 0.250 g resorcinol and 0.250 g NH_4Cl (Sartorius Secura124-1S analytical balance) are added into the emulsifier solution prepared in step (1) under magnetic stirring (IKEA® RCT digital magnetic stirrer, 300 rpm, 5 min). After a clear solution is obtained, its pH is monitored and carefully adjusted to 3.50 ± 0.02 with 1 M and 0.1 M HCl solutions (Mettler Toledo FiveEasy pH meter, LE407 electrode) under stirring; **(3)** ***core preparation*****:** a fluorescent compound (Nile red or Brooker's merocyanine dye) is dissolved in the corresponding core chemical at a concentration of 0.1 mg/mL in a capped glass vial via ultrasonication (VWR USC100T) for 10 min and a clear solution is obtained; **(4)** ***emulsification*****:** the stained core solution prepared in (3) is emulsified into the solution prepared in (2) with a high shear homogenizer (Silverson L4RT, Emulsor Screens with standard perforations, 1200 rpm, 20 min) in a 200 mL glass beaker. The core liquid is injected into the aqueous solution via a syringe with a TERUMO® AGANI™ 25G×5/8" (0.5×16 mm) needle (LUER 6% regular bevel); **(5)** ***polymerization*****:** the produced emulsion is transferred into a 250 mL jacketed beaker (Sigma-Aldrich UK, Aldrich Z137065, with a customized baffle) connected with a water bath (Julabo ME-F25, circulating water as a coolant). The emulsion is agitated with a Rushton turbine (IKA R3001) on a mechanical stirrer (IKA Eurostar Labortechnik, 600 rpm). 6.5 mL formaldehyde is injected into the agitated emulsion, after which the beaker opening is covered with aluminum foil to prevent evaporation during polymerization. The connected water bath is programed as described: the temperature is maintained at 20 °C for 30 min, then ramped up to 55 °C at 1 °C/min and maintained at 55°C for 4 h. Temperature is then programed to return to 20 °C at -1 °C/min; **(6)** ***Washing*****:** once temperature returns to 20 °C, the final product is transferred into 3× 50 mL centrifugation tubes, centrifuged (Labnet centrifuge, Hermle Labortechnik GmbH, 6000 rpm for 5 min) 4 times, and vacuum filtered by 5 L of distilled water (KNF LAB LABOPORT Diaphragm vacuum pump, Büchner funnel, filter paper Fisherbrand 11435248 QL100). Washed capsules are re-dispersed and stored in distilled water and dried upon request.

For all capsules presented in **Figure 1**, gum Arabic was used as the emulsifier in step (1) of the protocol, and solution preparation was completed by adding 0.150 g gum Arabic into 150 g distilled water and keeping the solution under stirring (IKEA® RCT digital magnetic stirrer, 300 rpm, 15 min). The corresponding core chemicals 1-octene, Dotherm J, toluene, benzyl benzoate and 1-octanol stained with Nile red were used respectively in step (3) to produce capsules with

different cores presented in Figure 1. All other parameters were identical as described in the protocol.

For all capsules presented in **Figure 2**, heptane stained by Nile red was used as the core. Batch 1 capsules were produced with poly(vinyl alcohol) as the emulsifier in step (1). 0.150 g poly(vinyl alcohol) was dissolved into 150 g distilled water by stirring at 85 °C (IKEA® RCT digital magnetic stirrer with a PT 1000.80 temperature sensor, 300 rpm, 5 h, 200 mL capped glass bottle with a drilled hole for temperature sensor) and cooled down naturally. All other parameters remained identical as described in the protocol. Batch 2 capsules were produced with gelatin-grafted graphene oxide as the emulsifier in step (1). In order to prepare the emulsifier solution, 0.015 g gelatin was dissolved in 150 g distilled water by heating at 50 °C (IKEA® RCT digital magnetic stirrer with a PT 1000.80 temperature sensor, 300 rpm, 1 h, 200 mL capped glass bottle with a drilled hole for temperature sensor) and cooled down naturally. 2.5 mL graphene oxide dispersion in water (2 mg/mL) was added into the prepared gelatin solution and ultrasonicated for 30 min. The dispersion was then transferred into a 250 mL flat bottom round flask and heated at 95 °C under stirring (IKEA® RCT digital magnetic stirrer with a PT 1000.80 temperature sensor, 500 rpm, 18 h, reflux setup with a glass condenser at cooling temperature 10 °C, Julabo ME-F25 with circulating water as a coolant), and then cooled down naturally. All other parameters remained identical. Batch 3 capsules were produced with gelatin alone as the emulsifier in step (1). The emulsifier solution was prepared by adding 0.015 g gelatin into 150 g distilled water and stirring the solution at 50 °C (IKEA® RCT digital magnetic stirrer with a PT 1000.80 temperature sensor, 300 rpm, 1 h, 200 mL capped glass bottle with a drilled hole for temperature sensor) and then cooled down naturally. All other parameters remained identical.

Capsules shown in **Figure 3** were synthesized as follows: 0.015 g xanthan gum was added into 150 g distilled water in a 200 mL glass beaker. High shear homogenization (Silverson L4RT, Emulsor Screens with standard perforations, 3000 rpm, 5 min) was performed to hydrate the gum in step (1) of the protocol. Hexadecane stained by Nile red was prepared as the core cargo in step (3). All other parameters remained identical.

Capsules presented in **Figure S1** were produced with gum Arabic as the emulsifier in step (1). 0.150 g gum Arabic was dissolved in 150 g distilled water by magnetic stirring (IKEA® RCT digital magnetic stirrer, 300 rpm, 10 min). Nile red stained isobutyl acetate was prepared as the

core cargo in step (3), with all other parameters being identical as described in the protocol. Capsules presented in **Figure S2** were produced with gum Arabic as the emulsifier in step (1). 0.150 g gum Arabic was dissolved in 150 g distilled water by magnetic stirring (IKEA® RCT digital magnetic stirrer, 300 rpm, 10 min). Brooker's merocyanine dye stained 1-octanol was prepared as the core cargo in step (3). The continuous phase was also stained with the same dye to alleviate diffusion of the dye out of the core during synthesis due to its water solubility. Final harvested capsules were washed thoroughly with 10 L water to remove the dye adsorbed at the exterior surface from the continuous phase. All other parameters were identical as described in the protocol. Capsules shown in **Figure S3** were produced with (+)-arabinogalactan from larch wood. The emulsifier solution was prepared by dissolving 0.150 g arabinogalactan in 150 g distilled water via magnetic stirring (IKEA® RCT digital magnetic stirrer, 300 rpm, 10 min) in step (1). Nile red stained heptane was prepared as the core cargo in step (3), with all other parameters being identical as described in the protocol.

***Capsule Synthesis – Solvent Extraction*: (1) *emulsifier solution preparation*:** two different emulsifiers were employed for the solvent extraction method. For poly(vinyl alcohol) solution preparation, 0.150 g Poly(vinyl alcohol) was dissolved into 150 g distilled water by stirring at 85 °C (IKEA® RCT digital magnetic stirrer with a PT 1000.80 temperature sensor, 300 rpm, 5 h, 200 mL capped glass bottle with a drilled hole for temperature sensor) and cooled down naturally. For sodium dodecyl sulfate solution preparation, 0.150 g sodium dodecyl sulfate was dissolved into 150 g distilled water by magnetic stirring at room temperature (IKEA® RCT digital magnetic stirrer, 300 rpm, 30 min); **(2) *core preparation*:** 2.500 g poly(methyl methacrylate) was weighed and transferred into a 100 mL glass bottle. The powder was spread out at the bottom of the bottle to prevent agglomeration upon contact with the solvent in order to achieve good dissolution quickly. 70 g dichloromethane (DCM) was weighed and poured into the glass bottle. The bottle was then capped and placed inside an ultrasonic bath until a clear solution was formed. The solution was then stored inside a fridge (4 ℃) to cool down. 4.2 g hexadecane stained by Nile red was then mixed into the prepared solution and ultrasonicated again until a clear solution was formed. The solution was again stored in a fridge (4 ℃) to cool down; **(3) *emulsification and solvent evaporation*:** the cooled solution prepared in step (2) was emulsified into the two solutions separately in step (1) inside a 250 mL jacketed beaker connected with a water bath maintained at 20 ℃ (Julabo ME-F25, water as coolant) on a high

shear homogenizer (Silverson L4RT, Emulsor Screens with standard perforations, 1600 rpm, 1 h). The temperature was then ramped up to 35 ºC at 1 ºC/min and maintained at 35 ºC for 1 h; **(4)** ***centrifugation*:** the product was then centrifuged once (Labnet centrifuge, Hermle Labortechnik GmbH, 6000 rpm for 5 min) without further washing.

The dried capsules presented in **Figure S6 (a)** and the core-shell-structured capsules dispersed in water shown in **Figure S6 (d)** were produced by using poly(vinyl alcohol) as the emulsifier in step (1). The solid poly(methyl methacrylate) particles presented in **Figure S6 (b)** were produced by removing the core hexadecane from step (2). The acorn-shaped capsules dispersed in water shown in **Figure S6 (d)** were produced by using sodium dodecyl sulfate as the emulsifier in step (1).

***Bright-Field Optical (OM) and Fluorescence Microscopy (FM)*:** bright-field optical microscopy images were captured on a Leica DMRBE microscope with PL FLUOTAR 5×/0.12 and 10×/0.30 objective lens. The fluorescent emission colors of capsules under excitation were also captured on the Leica microscope with a CoolLED pE-300 series illumination system. A blue light source was selected for the excitation with its maximum at around $\lambda_{ex\ max}$ = 460 nm. A H3 filter cube (BP420-490) with a dichromatic mirror (510) and suppression filter (LP 515) was selected as the configuration. Samples were dispersed via a pipette onto clean glass slides, spread out into a thin liquid film by tilting the slide, and dried under ambient conditions for observation. Digital images were captured with a Motic® CCD252 camera and snapped with Motic® Images Advanced 3.2 software.

***Scanning Electron Microscopy (SEM)*:** SEM micrographs were captured on a Hitachi TM3030 electron microscope with a backscattered electron (BSE) detector in EDX mode. Capsules were firstly dried into powders and then sprinkled onto carbon adhesive pads attached to aluminum stubs. Loosely attached particles were blown off with an air gun. Samples were then coated with a 5 nm gold layer (Quorum Q150R ES rotary-pumped sputter coater) to reduce electron accumulation. The charge-up reduction mode was used to further reduce artefacts caused by charging.

***Fluorescence Spectroscopy*:** capsules were dispensed in an aqueous medium onto microscope glass slides and immobilized with cover glasses. The glass slides with capsules were then placed

onto the stage of a Nikon A1R confocal system equipped with an Eclipse Ti microscope and a multiline laser bed. Particularly, the emission spectra for all capsules were captured uing a monochromatic laser at a wavelength of 488 nm generated at 40 mW and a 32-array spectral PMT detector with a Galvano scanner where the pinhole size was set to 49.8 µm. The microscope configuration used for the experiments included a BS20/80 dichroic mirror and an open band-pass filter.

***Thermogravimetric Analysis (TGA)*:** TG signals were recorded on a Linseis STA instrument. Capsules were firstly dried into flowing powders without agglomeration. 3/4 volume of a 0.14 mL Al_2O_3 crucible was filled by the dry powders and placed in the sample position on the TG-DSC heat flux sensor inside a high-temperature furnace with a type-K thermocouple sensor. A same type of empty Al_2O_3 crucible was used as the reference on the TG-DSC heat flux sensor. Sample weights were obtained on a Mettler Toledo EXCELLENCE Plus XP6U analytical balance and used for normalization. The furnace temperature was maintained at 25 ºC for 5 h and the sample chamber was flushed with Ar gas at a flow rate of 10 mL/min. A blank test at the same experimental conditions was performed first and the TG signal was stored as the baseline to be subtracted from any further tests for samples.

***Gas Chromatography-Mass Spectrometry (GC-MS)*:** A calibration curve was first established with a set of known concentrations of heptane in nonane mixtures. These mixtures were prepared by pipetting (Eppendorf Research 10 (0.5 – 10 µL) and Eppendorf Research 200 (20 – 200 µL) pipettes) 1, 5, 10, 20, 50 and 75 µL heptane into 1 mL volumetric flasks (Volac® mini-volumetric flask, 1 mL volume, accuracy ± 0.025 mL) and topping them up with nonane to the marked liquid levels equivalent to 1 mL. The mixtures were then slowly pumped for a short period of time with disposable pipettes in order to achieve uniform blending and then transferred quickly into GC glass vials and sealed (Agilent, 2 mL screw top borosilicate glass vials and caps with PTFE/silicone septa). These mixtures of known concentrations were tested on an Agilent GC/MSD 6890N/5873N system with a 190915-433 capillary column (HP-5MS, 0.25 mm (nominal diameter) × 30 m (nominal length) × 0.25 µm (nominal film thickness)). The analyte injection volume was 1 µL from a 10 µL syringe at a split ratio of 1:250. The oven was set to an initial temperature of 50 ºC for 5 min and then ramped up to 150 ºC for 5 min during extraction. Flow rate was 1 mL/min in constant flow mode and the carrier gas was helium. The mass

spectrometer was in single ion monitoring (SIM) mode and the target ion mass was 100. A linear relationship between heptane concentration in nonane and the peak area was established. Further testing heptane in nonane mixtures of unknown concentrations would yield a peak of known area, corresponding to an equivalent concentration on the linear calibration curve. Heptane extraction from capsules was carried out by crushing them inside a GC glass vial with 1 mL syringe plungers and then adding nonane for extraction. Filtration through a syringe filter with PTFE membrane (VWR 514-0071, pore size 0.45 μm) was carried out to prepare the final analytes. Three replicates were performed for each sample.

***Differential Scanning Calorimetry (DSC)*:** the phase transition of hexadecane-PUF capsules was analyzed by capturing DSC thermogram within −40 ~ 40 ºC on a Mettler Toledo DSC 2 STAR^e system. Capsules were firstly vacuum filtered and dried on filtering paper at ambient conditions for 1 h into flowing powders. A weighed amount of powder (Mettler Toledo Excellence Plus XP6U analytical balance) was then transferred inside a 40 μL aluminum crucible with a lid and sealed by a sealing press (Mettler Toledo A2). The crucible lids were without hole punctures. Three replicates were performed for the DSC test. A same type of sealed empty crucible was used as the reference. Samples were automatically inserted by the instrument robot into the furnace. The program profile was as follows: temperature rose from room temperature to 40 ºC and maintained at this temperature for 5 min. It then reduced to -40 ºC at a cooling rate of -2 ºC/min and maintained at -40 ºC for 5 min. Afterwards, the temperature rose up to 40 ºC again at a heating rate of 2 ºC/min.

***Temperature Control*:** the temperature control for the phase change observation of hexadecane-PUF capsules demonstrated in Figure 3 was performed with a complete Linkam T95-PE system controller (Peltier stage). A 2 L liquid nitrogen dewar connected with a LNP95 pump was used to cool down the chamber at a cooling rate of -2 ºC/min. The heating rate was set 2 ºC/min. The Linkam chamber was positioned on the stage of the Leica DMRBE microscope under the same setup as described above. Hexadecane-PUF capsules were dried into a free-flowing powder and then sprinkled onto a thin cover glass with an ultrathin double-sided tape (Tesa® 68557 10 μm d/s ultrathin PET tape by courtesy of Tesa®) to permit transmission. The cover glass with adhering capsules was immobilized by double-sided tape on top of the stainless steel surface with underneath circulating liquid nitrogen. The chamber cap with an observation window was

then screwed back on. A PL FLUOTAR 5×/0.12 objective lens was used for observation, which was the maximum magnification objective allowed due to the limited working distance. The nitrogen gas-out tube was placed on top of the chamber cap near the observation window blowing nitrogen to reduce condensation from the air at low temperatures. Bright-field and fluorescent microscopy micrographs were captured by alternating between white light and blue excitation light illumination.

Results and Discussion

Figure S1 illustrates the emission colors of dried capsules loaded with isobutyl acetate and crushed ones. Owing to a similar polarity, capsules emitted an orange color like benzyl benzoate. Due to the higher volatility of isobutyl acetate (boiling point 118 ºC, vapor pressure 1.7 kPa at 20 ºC), its fast evaporation after capsule rupture left little solvent residue, rendering Nile red nonsolvated and a red color emission. The color contrast between loaded and unloaded capsules for this ester was still discernible orange-red. It was envisaged that benzyl benzoate should have had a resembling contrast if the core cargo had evaporated completely. In reality, as a result of the extremely low volatility of such a chemical (boiling point approx. 324 °C, vapor pressure <0.03 Pa at 20 ºC), remaining cargo molecules prolonged their interaction with the fluorophore and shifted the emission color hypsochromically compared with excitation in

air. This was the reason for the hardly distinguishable color contrast, different in nature from the 1-octanol scenario.

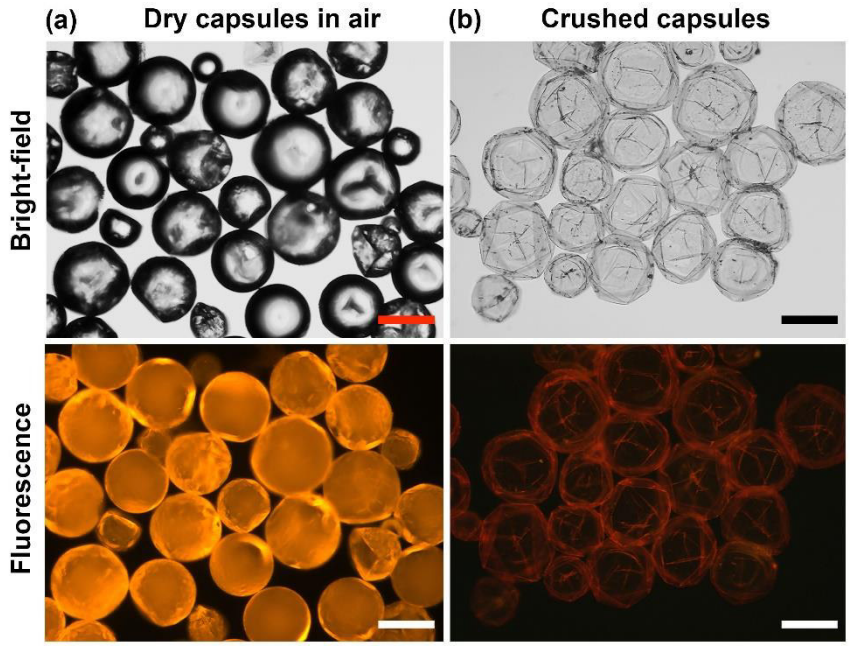

Figure S1 Orange-red fluorescent color switch for the retention-leakage detection of isobutyl acetate in PUF capsules stained by Nile red. Bright-field optical and fluorescence microscopy images (scale bars 100 μm) of (a) dry isobutyl acetate-PUF capsules in air emitting an orange fluorescent color; (b) unloaded PUF shells after crushing bearing no isobutyl acetate while emitting a red fluorescent color.

Figure S2 demonstrates the feasibility of restoring the color contrast between unloaded and loaded capsules with the alcohol cargo 1-octanol, by replacing Nile red with Brooker's merocyanine dye (MOED). Because of the positive solvatochromism of Nile red, an increasing polarity in core cargos produced a bathochromic shift in its emission wavelength, causing difficulty in differentiating loaded and unloaded capsules. Resorting

to a distinct fluorescent dye restored the color change for retention-leakage at the polar cargo end. It was not possible to test MOED in 1-octene, Dotherm J, toluene or benzyl benzoate on account of its limited solubility in these solvents.

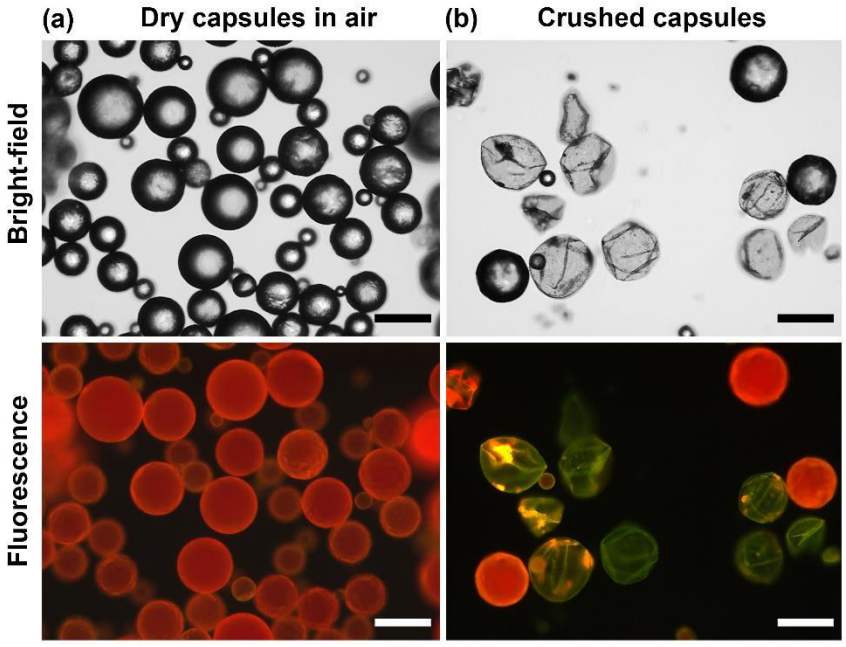

Figure S2 Red-green fluorescent color switch for the retention-leakage detection of 1-octanol in PUF capsules stained by Brooker's merocyanine dye (MOED). Bright-field optical and fluorescence microscopy micrographs (scale bars 100 µm) of (a) dry 1-octanol- PUF capsules in air emitting a red fluorescent color; (b) unloaded PUF shells after crushing emitting a green fluorescent color and intact 1-octanol- PUF capsules emitting a red fluorescent color.

Air bubbles would reduce capsule payload and may be detrimental for applications where a high payload of active core materials is preferred. The fluorescent staining concept also offers a good contrast to identify air bubbles during emulsification, in capsules dispersed in the continuous phase or in dry capsules as shown in Figure S3.

This potentially offers a method of differentiating air bubbles trapped in dry capsules from those with an immiscible second core liquid phase produced from double emulsions, where the fluorophore is also soluble.

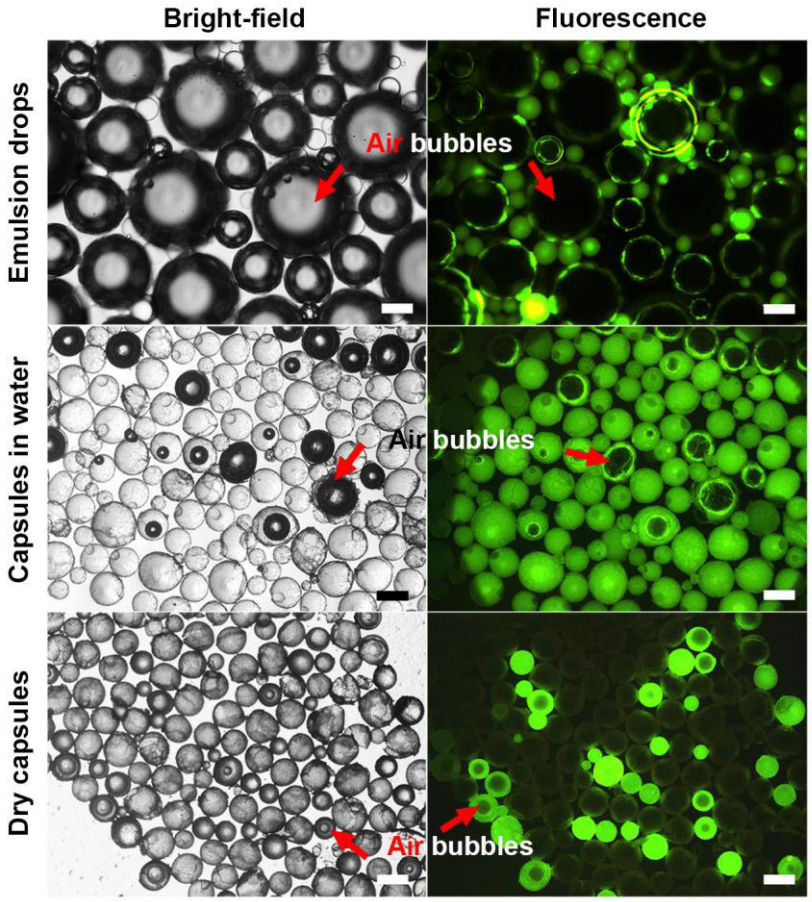

Figure S3 Identification of trapped air bubbles in a heptane-in-water emulsion and produced heptane-PUF capsules (scale bars 50 µm).

Figure S4 shows the morphology of capsules presented in Figure 2 of the main manuscript. The employed emulsifiers underlie the different release behaviors of corresponding capsules. When poly(vinyl alcohol) (PVOH) was used, a large quantity of

holes resided within shells contributing to the fast leakage of heptane. Switching from PVOH to gelatin-grafted graphene oxide (GO) apparently eliminated these holes from the shell structure and substantially improved the barrier property. Nevertheless, shell delamination suggested weaker cohesion within its structure compared with that produced by gelatin alone, which had the most compact and smoothest texture among the three samples. It is postulated that specific emulsifiers confer more compact shell structures with lower permeability via polymerization kinetics modification and additional chemical reactions.[1]

Figure S5 presents the various gray values between the highly bright and dim fluorescent regions corresponding to assorted fluorescent emission light intensities. The different numbers of emission photons collected at solvent-rich and solvent-deficient regions caused this intensity discrepancy.

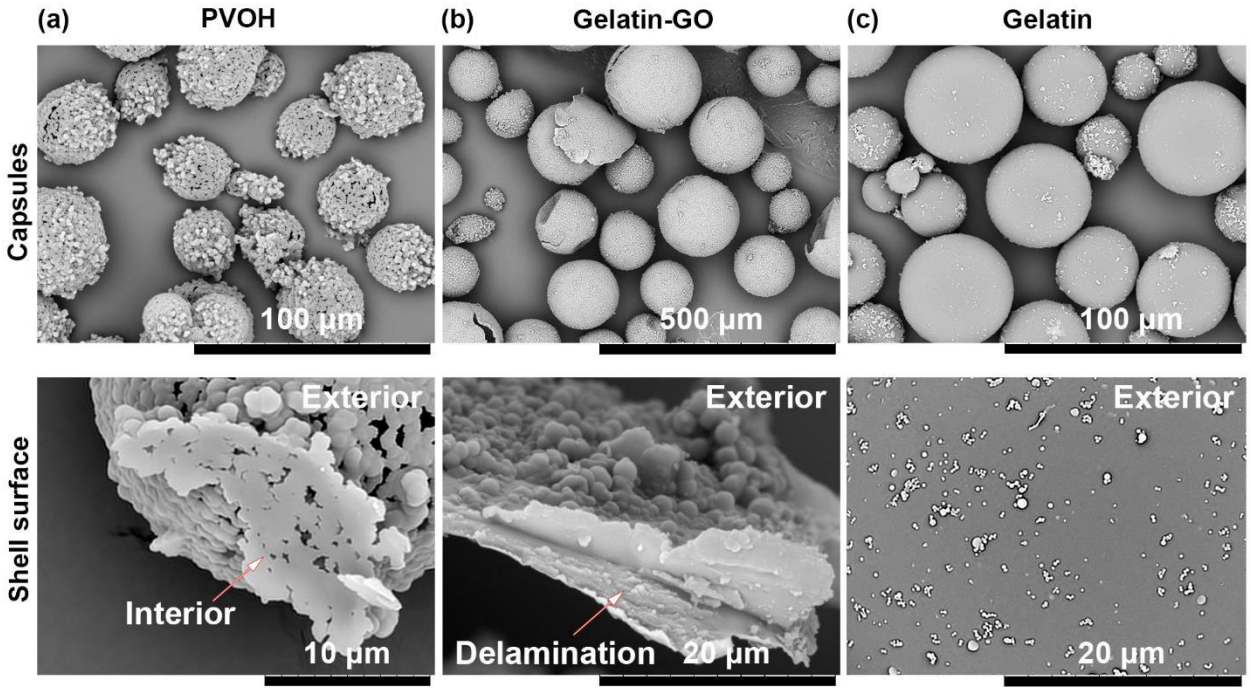

Figure S4 SEM micrographs of amino resin capsules loaded with heptane produced by (a) PVOH, (b) gelatin-GO, and (c) gelatin as an emulsifier with their surface morphology.

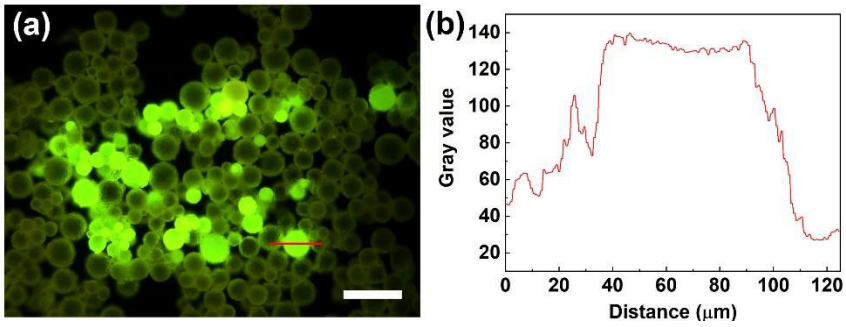

Figure S5 Gray values corresponding to the different emission light intensities in highly fluorescent and dim regions. (a) the 1 min aliquot in Figure 2a representing the moment of an incomplete ongoing leaking process (white scale bar 100 μm); (b) the grey value difference acquired in ImageJ across the highly bright and dim regions denoted by the red line in (a).

Figure S6 (a) and (b) demonstrate that it is not possible to differentiate the two samples produced via solvent extraction. When we synthesized these two samples, one of them

was deliberately formed as solid particles without adding any core cargo. The other one was synthesized as usual intending to produce core-shell structured capsules with Nile red stained hexadecane as the cargo. SEM and bright-field microscopy failed to differentiate them, and additional compositional analysis would be required. The fluorescence method offers a good nondestructive solution here to this problem. The green emission color from Nile red in hexadecane under excitation succeeded in confirming that Figure S6 (a) was actually successful core-shell capsules. While the other sample in Figure S6 (b) was identified as solid particles without liquid cores with a red fluorescence emission color.

The fluorescence sensing concept can also provide insights early into the synthesis process before encapsulation is even completed. For instance, for the solvent extraction process, during evaporation of the good solvent and phase separation for the shell formation, fluorescence proved to be useful in emulsion drop structure identification. It is well known that selected emulsifiers could result in either acorn- or core-shell-structured emulsion drops in solvent extraction depending on how they change the interfacial tension relationships within the whole system.[2-3] In order to encapsulate liquids, acorn-

structured emulsion drops must be avoided. We adopted two different emulsifiers, sodium dodecyl sulfate (SDS) and PVOH, in an attempt to encapsulate hexadecane inside poly(methyl methacrylate) (PMMA). Only PVOH showed success in fulfilling this purpose as shown in Figure S6 (a) after drying. When observing the emulsion drops during the formulation process, we could see the initial core-shell structure in Figure S6 (d)-4. On the other hand, SDS produced only acorn-shaped drops with hexadecane and PMMA separating out next to each other instead of PMMA wrapping around hexadecane (Figure S6 (d)-2). Even though bright-field microscopy could clearly identify the acorn structure (Figure S6 (d)-1), it failed to confirm the core-shell configuration (Figure S6 (d)-3). Fluorescence microscopy distinguished both structures on the other hand. One can accordingly determine easily if selected emulsifiers are appropriate for the encapsulation process at an early stage without studying interfacial tension or sketching tertiary phase diagrams.

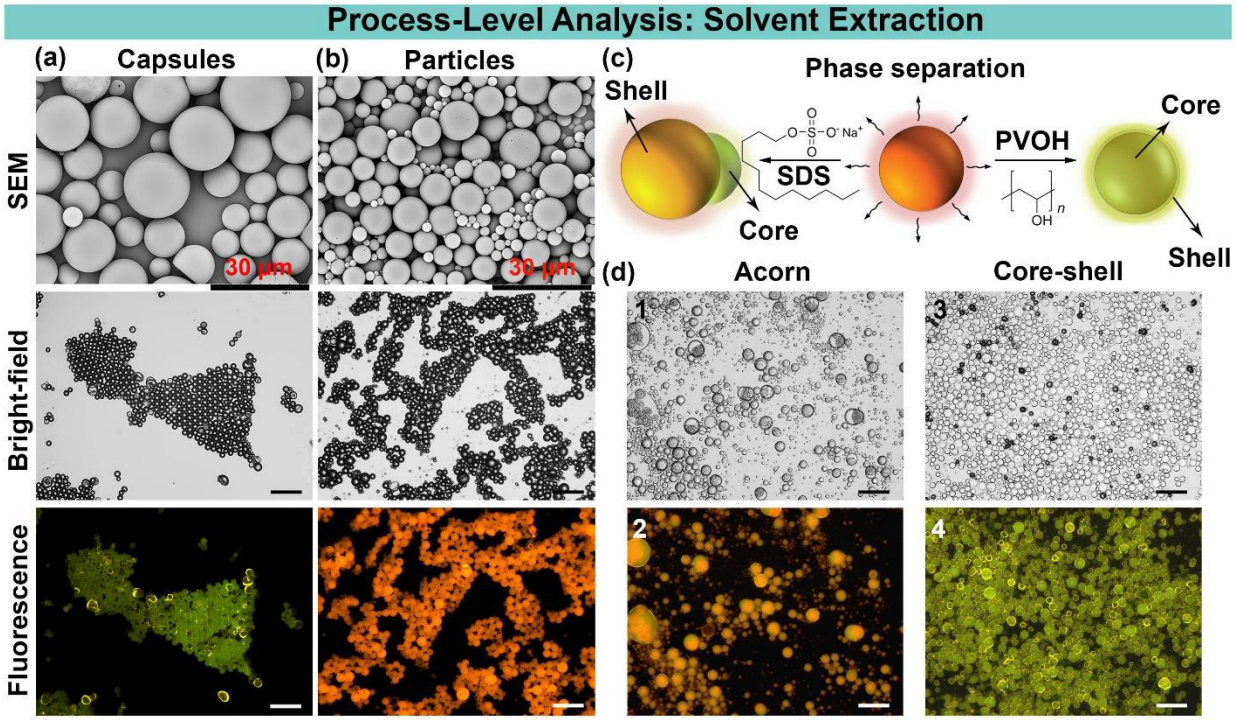

Figure S6 Process-level analysis: solvent extraction. Differentiation via fluorescence between (a) hexadecane-PMMA capsules and (b) solid PMMA particles; (c) schematic illustration of the different structures formed with sodium dodecyl sulfate (SDS) and poly(vinyl alcohol) (PVOH) as emulsifiers; (d) acorn and core-shell structures observed under bright-field and fluorescence microscopy during the formulation process of solvent extraction in the aqueous phase with SDS and PVOH as the emulsifier, respectively (all scale bars 100 μm unless specified otherwise).

References

(1) Zhang, Y.; Jiang, Z.; Zhang, Z.; Ding, Y.; Yu, Q.; Li, Y. Polysaccharide Assisted Microencapsulation for Volatile Phase Change Materials with a Fluorescent Retention Indicator. *Chem. Eng. J.* **2019,** *359* (10), 1234-1243.

(2) Loxley, A.; Vincent, B. Preparation of Poly(methylmethacrylate) Microcapsules with Liquid Cores. *J. Colloid Interface Sci.* **1998,** *208* (1), 49-62.

(3) González, L.; Kostrzewska, M.; Baoguang, M.; Li, L.; Hansen, J. H.; Hvilsted, S.; Skov, A. L. Preparation and Characterization of Silicone Liquid Core/Polymer Shell Microcapsules via Internal Phase Separation. *Macromol. Mater. Eng.* **2014,** *299* (10), 1259-1267.